

See discussions, stats, and author profiles for this publication at: <https://www.researchgate.net/publication/272044119>

# The 3D imaging and metrology of CMSX-4 superalloy microstructure using FIB-SEM tomography method

Article in *Solid State Phenomena* · February 2013

DOI: 10.4028/www.scientific.net/SSP.197.89

CITATIONS

6

READS

685

3 authors:



**Adam Kruk**

AGH University of Science and Technology in Kraków

91 PUBLICATIONS 759 CITATIONS

[SEE PROFILE](#)



**B. Dubiel**

AGH University of Science and Technology in Kraków

77 PUBLICATIONS 782 CITATIONS

[SEE PROFILE](#)



**A. Czyrska-Filemonowicz**

AGH University of Science and Technology in Kraków

241 PUBLICATIONS 3,474 CITATIONS

[SEE PROFILE](#)

## The 3D imaging and metrology of CMSX-4 superalloy microstructure using FIB-SEM tomography method

Adam Kruk<sup>a</sup>, Beata Dubiel<sup>b</sup> and Aleksandra Czyrska-Filemonowicz<sup>c</sup>

AGH University of Science and Technology, International Centre of Electron Microscopy for Materials Science and Faculty of Metals Engineering and Industrial Computer Science,  
Al. A. Mickiewicza 30, 30-059 Kraków, Poland

<sup>a</sup>kruczek@agh.edu.pl, <sup>b</sup>bdubiel@agh.edu.pl, <sup>c</sup>czyrska@agh.edu.pl

**Keywords:** FIB-SEM tomography, CMSX-4 superalloy, turbine blade

**Abstract.** STEM-EDX and FIB-SEM tomography studies have been carried out to visualize three-dimensional morphology of the  $\gamma'$  precipitates in different zones of ex-service turbine blade made of CMSX-4 single crystal superalloy. The results allowed the three dimensional analysis of the changes in microstructure of blade as resulting of operating conditions. Tomographic reconstructions provided quantitative data about  $\gamma$  and  $\gamma'$  phase shape, size and volume fraction. It was shown that FIB-SEM tomography technique is suitable for 3D reconstruction of the objects of 100 nm in size or even smaller and thus enables the accurate quantitative microstructural analysis of this superalloy.

### Introduction

The CMSX-4 single crystal (SC) nickel-base superalloy is widely used for gas turbine blades due to the superior creep and thermomechanical fatigue strength at temperature as high as 85% of its melting point. Its microstructure is especially tailored to ensure the high microstructure stability and the high temperature strength and consists of a high volume fraction (about 70 volume percent) of cuboidal  $\text{Ni}_3\text{Al}$ -base intermetallic  $\gamma'$  precipitates separated by Ni-base  $\gamma$  solid solution matrix in the form of nanometric width channels. When single crystal superalloys are subjected to stress at elevated temperature ( $T > 900^\circ\text{C}$ ), the microstructural instability called rafting occurs. Initially cuboidal  $\gamma'$  particles transform into plates [1 - 3]. It is evident from numerous experimental and theoretical investigations, that rafting is strongly controlled by the sign of applied stress, lattice misfit and differences in elastic constants between  $\gamma$  and  $\gamma'$  phases. Under high temperature creep conditions, the occurrence of rafting in single crystal superalloys is basically due to stress-assisted diffusion controlled process and the kinetics of rafting is dependent on the test temperature and duration.

Many studies performed by means of TEM and SEM methods provided the quantitative information about the  $\gamma$  and  $\gamma'$  phases in CMSX-4 [4 - 6]. However, most of them were based on metrology of the 2D projections of the 3D objects. During the last decade, the three-dimensional characterisation of materials has gained increasing attention due to the development of new tomographic techniques based on synchrotron radiation, X-rays or electrons [7 - 12]. These techniques apply 3D reconstructions of a series of transmitted or back scattered projections of a sample. X-ray transmission is non-destructive and produces absorption contrast of different phases, cracks and pores. Contrast imaging can be applied to visualize phase boundaries even in the absence of absorption contrast. The spatial resolution of synchrotron radiation facilities, which mainly depends on the effective pixel size of the detector, has reached the level of tenths of a micrometre.

The electron tomography is a relatively new technique that uses a Transmission Electron Microscopy (TEM) or Focused Ion Beam - Scanning Electron Microscopy (FIB-SEM) to 3D imaging of microstructure of engineering materials. The TEM tomography using High Angle Annular Dark Field Scanning Transmission Electron Microscopy (STEM-HAADF) or Energy Filtered Transmission Electron Microscopy (EFTEM) imaging methods was developed to reconstruct objects in three dimensions (3D) from a tilt series of 2D TEM images [8]. This technique is well accepted in the life science as a method used to study viruses or cells as well as for

visualization and metrology of structural elements in metallic alloys. The resolution in the 3D reconstructions, however, is limited to a few nanometres. The FIB-SEM tomography has become an important tool in materials science for studying of materials at the micro- and nanometre scale. The technique, due to its ability to perform precise in-situ milling, has been extended to studying 3D structural and chemical relationships. With the help of computer algorithms for processing data and graphics packages for display, 3D systems can be easily reconstructed and the structure interrogated to obtain both qualitative and quantitative information. It is possible to study features at spatial resolutions at the tens-of-nanometers level and volumes with dimensions of up to tens of microns. This allows the reconstruction of many systems in the size range important to nanotechnology.

The present work shows the results of application of FIB-SEM tomography methods for qualitative and quantitative evaluation of the microstructure of CMXS-4 turbine blade after service in stationary gas turbine.

### Material and experimental procedure

The qualitative and quantitative microstructural analysis of CMXS-4 ex-service turbine blade after operation for 12 700 hours and 200 starts in industrial gas turbine were performed using TEM-EDX and FIB-SEM tomographic methods. CMXS-4 ex-service blade was supplied by SIEMENS Industrial Turbomachinery Ltd, Lincoln. Chemical composition of CMSX-4 superalloy is as follows (wt %): Ni - 8.4 Co - 6.4 Cr - 6.5 Ta - 6.4 W - 5.68 Al - 2.8 Re - 1.04 Ti - 0.58 Mo. The distribution of temperature and stress in the analysed regions of the blade was as follows: 997 °C/30 MPa at the blade tip, 927 °C/111 MPa at the middle of the blade height, 807 °C/189 MPa at the blade bottom. STEM and EDX analysis were performed using of a probe C<sub>s</sub> corrected Titan<sup>3</sup> G2 60-300 microscope with ChemiSTEM™ detection system. It enabled to acquire high spatial resolution and high count rate STEM-EDX elemental maps to examine chemical elements partitioning between  $\gamma$  and  $\gamma'$  phases. The FIB lamellas for STEM-EDX investigation were prepared using Zeiss NEON 40EsB CrossBeam. This dual beam workstation was also used for FIB-SEM tomography. Serial FIB cross-sections in-situ milling was performed by Ga-ion beam at parameters: 30 kV, 100 pA and aperture of 30  $\mu$ m. For each slice SEM images (image size: 1024 x 768 pixels, 8 bit grayscale, recording time for 1 slice ~60 sec.) were taken with EsB detector using low voltage of 1.7 kV. The acquired stack of images was transformed directly into a 3D data volume with a voxel resolution of 8×8×8 nm<sup>3</sup>. The 3D visualization of reconstructed volume for FIB-SEM tomography was performed using ImageJA 1.45b and Avizo Fire 6.3 software.

### Results and discussion

TEM analysis of the CMXS-4 in the bottom of the blade shown that the microstructure is similar to that of in as-received alloy and consists of the cuboidal precipitates of  $\gamma'$  phase in  $\gamma$  matrix (Fig. 1a).

The distribution of chemical elements revealed on STEM-EDX maps indicates that  $\gamma$  phase is enriched in Cr, Co, Re, Mo and Ni, whereas the  $\gamma'$  phase contains Al, Ti, Ta and Ni (Fig.1b). Variation in chemical composition between the  $\gamma$  and  $\gamma'$  phases made it possible to obtain the optimum contrast for recording a series of FIB-SEM tomographic images using EsB detector.

Fig.2 shows the microstructure at the blade bottom observed in SEM using EsB and SE detectors. The sample surface is perpendicular to the [001] direction in a single crystal. The method of sample preparation to record a tomographic series of 2D images is illustrated in Fig. 2b, which presents an example image from a series of 433 images (8-bit grayscale, file size of 217 MB) recorded with EsB detector at 1.7 kV accelerating voltage. Very small distance of 8 nm between successive recorded images allowed at the magnification used to obtain voxel size and thus the resolution of the 3D level of 8 x 8 x 8 nm<sup>3</sup>. BSE images exhibited a good contrast between the  $\gamma$  and  $\gamma'$  phase's, suitable for the tomographic reconstruction and visualization of the 3D reconstructed volume of CMSX-4 superalloy. The segmentation performed on the 2D images allowed the separation in reconstructed volume of 7.7 x 4.4 x 3.5  $\mu$ m<sup>3</sup> the  $\gamma'$  precipitates and  $\gamma$  channels.

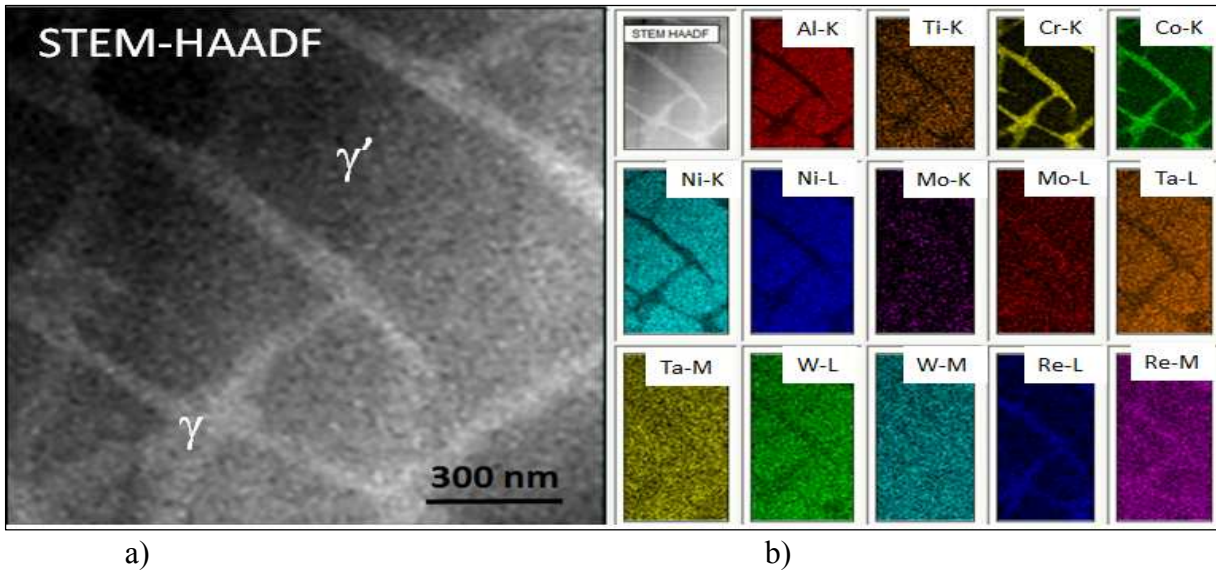


Fig. 1. Microstructure at the bottom of the CMSX-4 blade: a) STEM-HAADF image of  $\gamma'$  precipitates and  $\gamma$  matrix channels, b) STEM-EDX maps of chemical elements partitioning between  $\gamma$  and  $\gamma'$  phases.

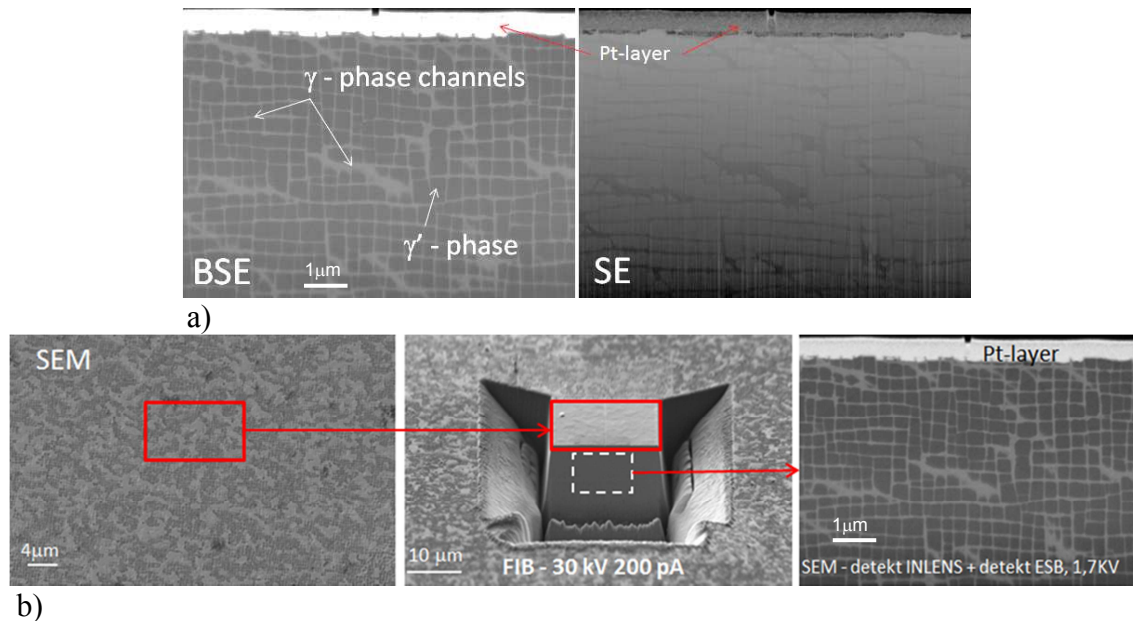


Fig. 2. Method of preparation of a sample area for recording tomographic series of images: a) comparison the microstructure of the tested alloy (from the blade bottom zone) imaged by SEM using BSE and SE detectors, b) selection of a location and method of tomographic imaging.

The microstructural changes of the CMSX-4 during service are more distinct in the middle and the tip of the investigated blade, both at the leading and trailing edge. In the middle zone, the well developed rafts oriented perpendicularly to longitudinal axis of the turbine blade are observed. At the blade tip the  $\gamma'$  plates are wavy, thicker and shorter than in the blade middle.

Figs 3 and 4 show the results of tomographic reconstructed and visualized in 3D analysed volume of samples taken from different blade zones (bottom, middle and tip). The 3D visualization of the reconstructed volume shows the spatial distribution of selected  $\gamma'$  precipitates in the  $\gamma$  matrix.



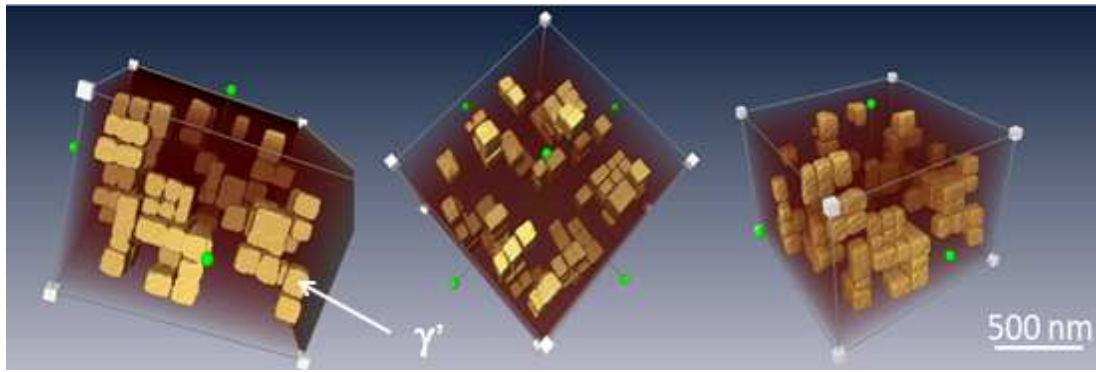


Fig. 3. The results of the 3D tomographic reconstruction of a volume of  $3.5 \times 3.5 \times 3.5 \mu\text{m}^3$  for CMSX-4 superalloy.

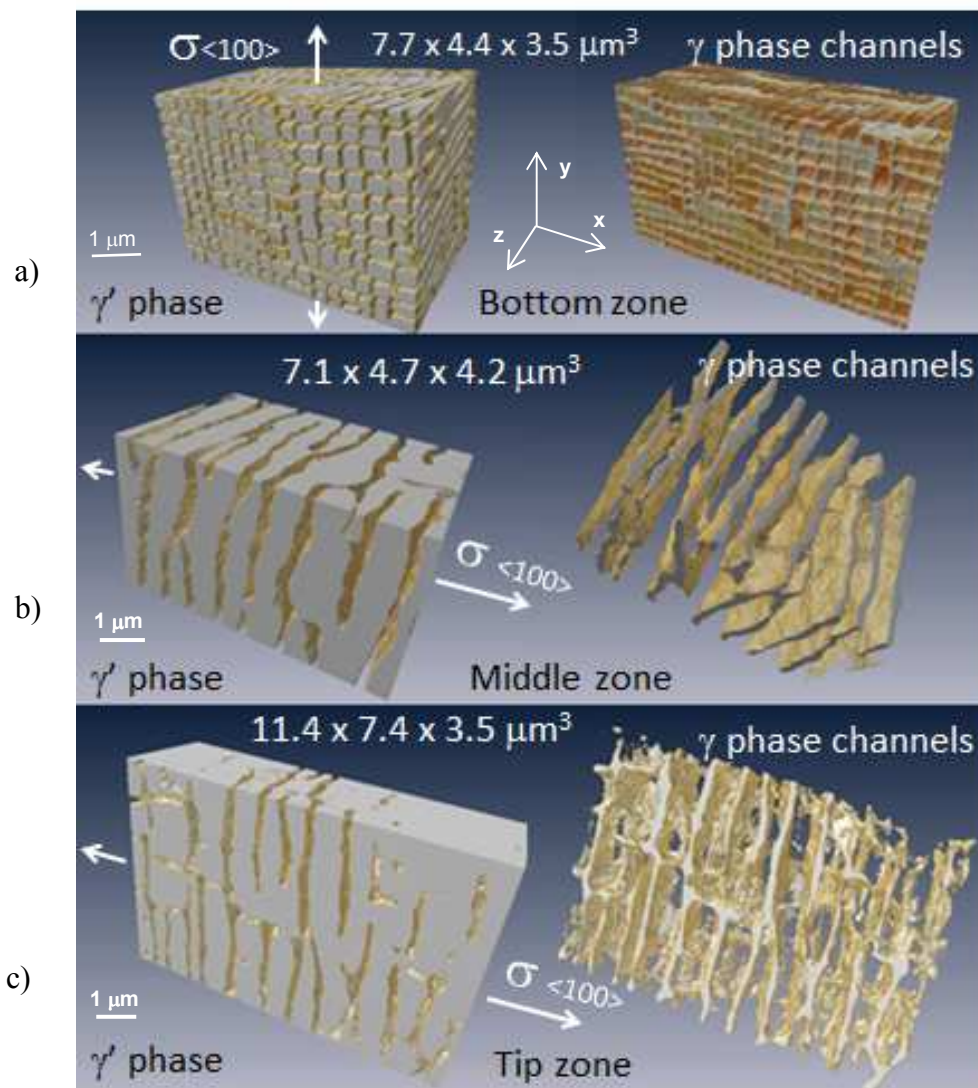


Fig. 4. Results of application FIB-SEM tomography method to 3D visualization of spatial distribution and shape of the  $\gamma'$  and  $\gamma$  phases in a) bottom, b) middle and c) tip zones of the CMSX-4 blade.

Quantitative evaluation of the width of  $\gamma$  phase channels appropriately oriented was carried out on the images after the application of digital image filtering using two-dimensional Fast Fourier

Transform (2D FFT). The performed digital filtration allowed the visualization on the image only those  $\gamma$  phase channels, whose orientation was determined. An example of 2D FFT application for image filtering is shown in Fig. 5.

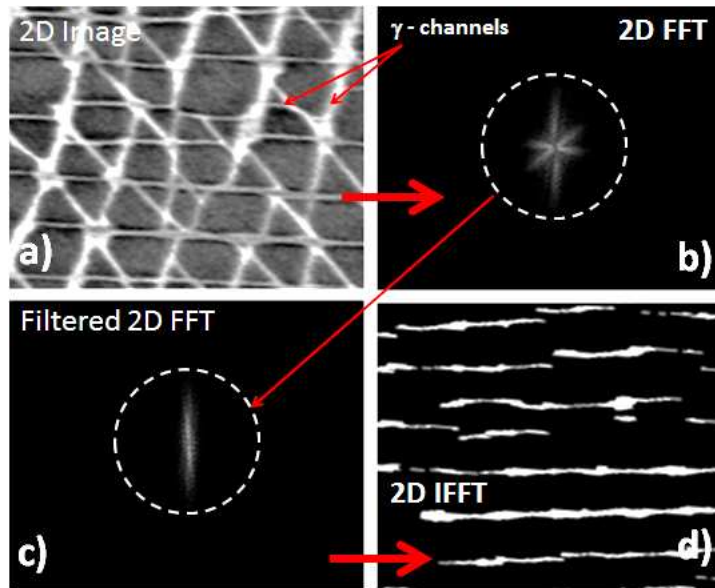


Fig. 5. Application of 2D FFT for image filtering: a) initial image with different orientation of  $\gamma$  channel, b) 2D FFT of image, c) filtered 2D FFT, d) inverse Fourier transform of filtered 2D FFT image.

On the basis of the reconstructed space, the volume fraction of  $\gamma'$  phase as well as the average width of  $\gamma'$  precipitates and  $\gamma$  channels were determined in the bottom, middle and tip zones of the blade. The results are shown in Table 1. At the bottom of the blade an average edge length and volume fraction of  $\gamma'$  phase are equal respectively  $293.3 \pm 125.8$  nm and  $71.9 \pm 1.5$  %. In the middle of the blade height an average width of  $\gamma'$  precipitates and  $\gamma$  channels parallel to the direction of the acting stress are equal to  $\gamma' = 503.5 \pm 77.5$  nm and  $\gamma = 163.4 \pm 21.8$  nm. Fig. 4c shows the visualisation of the microstructure at the tip of the blade. The partial decay of  $\gamma$  phase channels oriented parallel to the [010] and [001] directions can be observed. This fact illustrates the complex state of stress that occurred in the reconstructed sample volume at the tip of blade. The volume fraction of  $\gamma$  phase channels in the analysed volume at the tip of the blade is  $14.8 \pm 2.2$ %. Determined average width of the  $\gamma'$  phase precipitates and  $\gamma$  channels in the direction parallel to the direction [010] are equal to  $1044.7 \pm 29.5$  nm and  $155.3 \pm 29.5$  nm, respectively. These values are much larger than in the middle of the blade, where the pronounced rafting occurs. It can result from a coagulation of  $\gamma'$  precipitates with parallel dissolution of  $\gamma$  channels in the [010] direction.

Table 1. Microstructural parameters of CMSX-4 superalloy estimated from FIB-SEM tomographic reconstruction of sample volumes at the bottom, middle and tip zones of ex-service CMSX-4 blade

Blade zone	Temperature and stress conditions	Volume fraction of $\gamma'$ phase, $V_V$ [%]	Average width of the $\gamma$ phase channels, [nm]	Average width of the $\gamma'$ precipitates, [nm]
<b>Bottom</b>	807 °C/189 MPa	$71.9 \pm 1.5$	$75.5 \pm 10.1$	$293.3 \pm 125.8$
<b>Middle</b>	927 °C/111 MPa	$76.6 \pm 1.9$	$163.4 \pm 21.8$	$503.5 \pm 77.5$
<b>Tip</b>	997 °C/30 MPa	$85.1 \pm 2.2$	$155.3 \pm 29.5$	$1044.7 \pm 29.5$

## Summary

The quantitative analysis of tomographic reconstructed CMSX-4 superalloy by FIB-SEM tomography provided the significant information about the particle shape, spatial distribution as well as their size and volume fraction. The statistical error for the volume fraction in 3D depends on the size and shape of the analysed structure. The systematic error depends primarily on the lateral resolution of the characterization method and the image contrast. Due to the high resolution of FIB-SEM tomography and excellent contrast between the precipitates and the matrix in BSE images, the systematic error for the chosen resolution  $8 \times 8 \times 8 \text{ nm}^3$  for the analysed system can be neglected. FIB-SEM tomography results confirmed of CMSX-4 ex-service blade the advantage of this new technique for 3D imaging and metrology of engineering materials.

**Acknowledgements:** The financial support by the European Institute of Innovation and Technology, under the KIC InnoEnergy NewMat project (KIC NewMat, nr 7.7.110.7023) and Polish Ministry of Science and Higher Education (AGH project nr 11.11.110.148) is gratefully acknowledged. The authors acknowledge the SIEMENS Industrial Turbomachinery Ltd, Lincoln, UK for providing the material for investigation within COST Action 538. The authors also thank Mr A. Gruszczyński, MSc. for his assistance in the FIB-SEM investigation.

## References

- [1] P. Caron, T. Khan, Improvement of creep strength in a nickel base single crystal superalloy by heat treatment, *Mater. Sci. Eng.* 61 (1983) 173 - 184.
- [2] F.R.N. Nabarro, Rafting in Superalloys, *Met. Trans. A* 27 (1996) 513- 530.
- [3] M. Ziętara, PhD thesis, AGH University of Science and Technology, 2011.
- [4] M. Veron, Y. Brechet and F. Louchet, Strain induced directional coarsening in Ni-base superalloys, *Scripta Metall. Mater.* 34 (1996) 1883 - 1886.
- [5] V. Sass, U. Glatzel, M. Feller-Kniepmeier, Anisotropic creep properties of the nickel-base superalloy CMSX-4, *Acta Mater.* 44 (1996) 1967 - 1977.
- [6] B. Dubiel, A. Czyrska-Filemonowicz, Microstructural changes during creep of CMSX-4 single crystal Ni base superalloy at 750°C, *J. Microsc.* 237 (2010) 364-369.
- [7] A. Kruk, A. Czyrska-Filemonowicz, Contribution of electron tomography to development of innovative materials for clean energy systems and aeronautics, will be published in *Arch. Metall. Mater.*
- [8] P.A. Midgley and M. Weyland, 3D electron microscopy in the physical science: the development of Z-contrast and EFTEM tomography, *Ultramicroscopy* 96 (2003) 413 – 431.
- [9] A. Kruk, B. Dubiel, W. Osuch, G. Cempura, A. Czyrska-Filemonowicz, Application of electron tomography for three-dimensional imaging of micro- and nanoparticles in metal alloys, (in Polish), *Inżynieria Materiałowa* 30 (2010) 86 – 93.
- [10] P.J. Withers, X-ray nanotomography, *Mater. Today* 10 (2007) 26-34.
- [11] P. Cloetens, M. Pateyron-Salome, J.Y. Buffiere, G. Peix, J. Baruchel, F. Peyrin, M. Schlenker, Observation of microstructure and damage in materials by phase sensitive radiography and tomography, *J. Appl. Phys.* 81 (1997) 5878-5886.
- [12] S.R. Stock, 2008. Recent advances in X-ray microtomography applied to materials, *Int. Mater. Rev.* 53/3 (2008) 129-181.